bioRxiv preprint doi: https://doi.org/10.1101/2020.08.28.272492; this version posted August 29, 2020. The copyright holder for this preprint (which was not certified by peer review) is the author/funder, who has granted bioRxiv a license to display the preprint in perpetuity. It is made available under aCC-BY-NC-ND 4.0 International license.

Transcription coordinates histone amounts and genome content

Kora-Lee Claude[1], Daniela Bureik[1], Petia Adarska[1], Abhyudai Singh[2], Kurt M. Schmoller[1*]

[1]Institute of Functional Epigenetics, Helmholtz Zentrum München, 85764 Neuherberg, Germany

[2]Department of Electrical & Computer Engineering, University of Delaware, Newark, DE 19716, USA

*correspondence: kurt.schmoller@helmholtz–muenchen.de

Abstract

Biochemical reactions typically depend on the concentrations of the molecules involved, and cell survival therefore critically depends on the concentration of proteins. To maintain constant protein concentrations during cell growth, global mRNA and protein synthesis rates are tightly linked to cell volume. While such regulation is appropriate for most proteins, certain cellular structures do not scale with cell volume. The most striking example of this is the genomic DNA, which doubles during the cell cycle and increases with ploidy, but is independent of cell volume.

Here, we show that the amount of histone proteins is coupled to the DNA content, even though mRNA and protein synthesis globally increase with cell volume. As a consequence, and in contrast to the global trend, histone concentrations (i.e. amounts per volume) decrease with cell volume but increase with ploidy. We find that this distinct coordination of histone homeostasis and genome content is already achieved at the transcript level, and is an intrinsic property of histone promoters that does not require direct feedback mechanisms. Mathematical modelling and histone promoter truncations reveal a simple and generalizable mechanism to control the cell volume- and ploidy-dependence of a given gene through the balance of the initiation and elongation rates.

Introduction

Maintaining accurate protein homeostasis despite cell growth and variability in cell volume is essential for cell function. Most proteins need to be kept at a constant, cell-volume-independent

bioRxiv preprint doi: https://doi.org/10.1101/2020.08.28.272492; this version posted August 29, 2020. The copyright holder for this preprint (which was not certified by peer review) is the author/funder, who has granted bioRxiv a license to display the preprint in perpetuity. It is made available under aCC-BY-NC-ND 4.0 International license.

concentration. Since the amount of ribosomes and transcriptional machinery increases in proportion to cell volume, constant protein concentrations can be achieved through machinery-limited protein biogenesis, where protein synthesis depends on the availability of limiting machinery components and thus increases in direct proportion to cell volume[1,2]. While machinery-limited regulation can maintain constant concentrations of proteins, total mRNA, and individual transcripts[3–6], it poses a conundrum for histones. As components of nucleosomes, histones are likely needed at a constant protein-to-DNA stoichiometry, implying that their amount should increase with ploidy but be independent of cell volume. In other words, histone concentration, *i.e.* amount per volume, should increase with ploidy but decrease with cell volume. Since accurate histone homeostasis is crucial for fundamental biological processes[7–10] and to avoid toxic effects[11–13], cells use several layers of regulation by translation, transcription and degradation to tightly coordinate histone production with genome replication[14–16]. However, how cells produce histones in proportion to genome content, even though protein biogenesis is generally linked to cell volume remains unclear.

Here, we use budding yeast as a model to show that histone protein amounts are coupled to genome content, resulting in a decrease of histone concentration in inverse proportion with cell volume, and an increase in direct proportion with ploidy. We find that this specific regulation of histones is achieved at the transcript level and does not require direct feedback mechanisms. While our data suggest that 3'-to-5'-degradation by the nuclear exosome is necessary for the correct decrease of concentration with cell volume, we show that histone promoters alone are sufficient to couple transcript amounts to gene copy number rather than cell volume. Our results suggest that this differential regulation of histones can be achieved through template-limited transcription, where mRNA synthesis is limited by the gene itself and does therefore not increase with cell volume. This provides a general mechanism by which cells can couple the amount of a subset of proteins to genome content while most protein concentrations are maintained constant.

bioRxiv preprint doi: https://doi.org/10.1101/2020.08.28.272492; this version posted August 29, 2020. The copyright holder for this preprint (which was not certified by peer review) is the author/funder, who has granted bioRxiv a license to display the preprint in perpetuity. It is made available under aCC-BY-NC-ND 4.0 International license.

Results

Histone protein concentrations decrease with cell volume and increase with ploidy

Typically, total protein amounts as well as the amounts of individual types of protein increase roughly in direct proportion to cell volume to maintain constant concentrations. However, such regulation is inappropriate for histones, whose amount we predicted should be coupled to the cellular genome content instead. To test if this is the case, we chose the budding yeast histone *HTB2*, one of two genes encoding for the core histone H2B, as an example, because it can be fluorescently tagged without pronounced effects on cell growth. We endogenously tagged *HTB2* with the fluorescent protein *mCitrine* in a haploid strain, and measured cell volume and the amount of Htb2-mCitrine as a function of time in cycling cells by microfluidics-based live-cell fluorescence microscopy[17,18]. To obtain a large range of cell volumes, we grew cells on synthetic complete media with 2% glycerol 1% ethanol as a carbon source (SCGE). As expected[14], we find that Htb2 amounts are constant during early G1, rapidly double during S-phase and reach a plateau before cytokinesis (**Fig. 1a**). We then quantified the Htb2-mCitrine amounts in new-born cells directly after cytokinesis and find that the amount of Htb2-mCitrine is largely constant, independent of cell volume (**Fig. 1b**). To further test whether histone amounts are coupled to genomic DNA content rather than cell volume, we next analyzed a diploid strain in which both alleles of *HTB2* are tagged with *mCitrine*. Indeed, Htb2-mCitrine amounts in diploid cells are approximately a factor of two higher than in haploid cells (**Fig. 1b**). To more accurately compare Htb2 concentrations in haploids and diploids of similar volume, we sought to increase the overlapping range of observable volumes in both strains. For this purpose, we deleted the endogenous alleles of the G1/S inhibitor *WHI5* and integrated one copy of *WHI5* expressed from an artificial, β-estradiol-inducible promoter system[19] (**Fig. 1c**). Using this system, we were able to increase the mean volume of steady-state exponentially growing populations by up to three-fold through overexpression of Whi5 (**Fig. 1d**) without drastically affecting doubling times, budding indices or cell cycle distributions (**Supplementary Fig. 1**). We repeated the microscopy

bioRxiv preprint doi: https://doi.org/10.1101/2020.08.28.272492; this version posted August 29, 2020. The copyright holder for this preprint (which was not certified by peer review) is the author/funder, who has granted bioRxiv a license to display the preprint in perpetuity. It is made available under aCC-BY-NC-ND 4.0 International license.

experiments described above with the inducible-Whi5 haploid and diploid strains in the presence or absence of β-estradiol. Again, we find that Htb2-mCitrine amounts are only very weakly dependent on cell volume, but show a roughly two-fold increase in diploid compared to haploid cells (**Supplementary Fig. 2a**). Consistently, we find that the concentration of Htb2-mCitrine at birth in both haploid and diploid cells decreases strongly with cell volume (**Fig. 1e**). To quantify this decrease, we performed a linear fit to the double-logarithmic data, and defined the slope as the 'volume-dependence-parameter' (VDP). The observed VDPs of -0.87 ± 0.04 (haploids) and -0.97 ± 0.03 (diploids), respectively, are close to the value of -1 expected for proteins that are maintained at constant amount, resulting in a decrease of concentration with $c \sim 1/V$. In contrast, proteins that are maintained at constant concentration would show a VDP of 0.

In budding yeast, histones are known to be tightly regulated at several layers. In particular, some histone genes – but not *HTB2* – exhibit dosage compensation at the transcript level[20–22]. In addition, excess histones are known to be degraded[16]. In principle, a coupling of histone amounts to genomic DNA content could be achieved through such feedback mechanisms: For example, larger cells may produce histones in excess, and then degrade the surplus. Alternatively, direct feedback of histone protein concentration on transcription could ensure that histones are expressed only until the protein amount matches the genome content. To test whether direct feedback of histone amounts on transcription, translation, or degradation is necessary to couple histone production to genome content, we again focused on Htb2, because it was already shown to not exhibit dosage compensation at the transcript level[21]. We constructed an inducible-Whi5 diploid strain in which we deleted one of the two *HTB2* alleles, while the other allele is tagged with *mCitrine* (**Fig. 1f**). If feedback were responsible for the coupling of Htb2 amount to genome content, the remaining *HTB2-mCitrine* allele should at least partially compensate for the deleted allele. However, consistent with the absence of any feedback, we find that Htb2-mCitrine concentrations are reduced by factor of two in the hemizygous compared to the homozygous diploid (**Fig. 1g**, **Supplementary Fig. 2b**).

bioRxiv preprint doi: https://doi.org/10.1101/2020.08.28.272492; this version posted August 29, 2020. The copyright holder for this preprint (which was not certified by peer review) is the author/funder, who has granted bioRxiv a license to display the preprint in perpetuity. It is made available under aCC-BY-NC-ND 4.0 International license.

Moreover, at a characteristic volume of 60 fL, at which we find both haploid and diploid new-born cells, the concentration of Htb2-mCitrine in the hemizygous strain roughly equals the concentration in the haploid (**Fig. 1g**). While it is still possible that the reduced concentration of Htb2-mCitrine is compensated by an increased concentration of the other H2B copy Htb1, our results suggest that no direct feedback is required to couple Htb2 amounts to genome content. Instead, Htb2 amounts are intrinsically determined by the *HTB2* gene copy number, independent of ploidy and cell volume.

Histone mRNA concentrations decrease with cell volume

The fact that the decrease of histone protein concentrations with cell volume is not simply a consequence of feedback, for example through excess protein degradation, suggests that it might already be established at the transcript level. To test if this is the case, we again employed the Whi5-overexpression system to measure the cell-volume-dependence of transcript concentrations (**Fig. 2a**). Specifically, we grew wild-type haploid cells, as well as the inducible-Whi5 haploid cells at three different β-estradiol concentrations (0, 10 and 30 nM), on SCGE media, which lead to a roughly four-fold range in mean cell volumes ranging from 39 ± 4 fL to 143 ± 21 fL (**Supplementary Fig. 3a**). To ensure steady state conditions, we grew cells for at least 24 hours at the respective β-estradiol concentration, before then measuring cell volume distribution, extracting total RNA, and performing reverse-transcription-qPCR (RT-qPCR). First, we measured the concentration of the ribosomal RNA *RDN18* relative to total RNA and found it to be constant (**Supplementary Fig. 4a**). This is consistent with the fact that ribosomal RNA constitutes the large majority of total RNA[23], which itself is expected to increase in direct proportion to cell volume[24] and allows us to now normalize other RT-qPCR measurements on *RDN18*.

Next, we quantified the mRNA concentrations of *ACT1* and *ENO2*, two genes that we expect to be expressed in proportion to cell volume such that the mRNA concentration are maintained constant. Indeed, we find that the VDPs for both transcripts are not significantly different from 0 (**Fig. 2b & d,**

bioRxiv preprint doi: https://doi.org/10.1101/2020.08.28.272492; this version posted August 29, 2020. The copyright holder for this preprint (which was not certified by peer review) is the author/funder, who has granted bioRxiv a license to display the preprint in perpetuity. It is made available under aCC-BY-NC-ND 4.0 International license.

Supplementary Fig. 4b). Interestingly, as previously suggested[25] we observe a slight decrease in concentration for the transcripts of the RNA polymerase II subunits *RPB1* and *RPB3* with increasing cell volume (**Fig. 2d, Supplementary Fig. 4c**)**.** We then quantified the concentrations of the transcripts of all core histone genes as well as the H1-like histone *HHO1*. In budding yeast, all core histone genes are present as two copies and expressed from bidirectional promoters controlling pairs of *H2A-H2B*[26] or *H3-H4*[27], respectively. Since the two copies of each core histone show high sequence similarity, we performed additional tests using deletion strains where possible to ensure qPCR primer specificity (**Supplementary Table 2**). We find that all histone transcripts show a significant decrease in concentration with cell volume, which is specific to the Whi5-dependent cell volume increase (**Supplementary Fig. 3b – d).** The histone mRNAs mostly exhibit VDPs close to -1 (**Fig. 2c & d, Supplementary Fig. 4d**). Thus, histone mRNA concentrations decrease with cell volume to ensure constant amounts – in contrast to global transcription, which increases with cell volume.

Hir1-dependent feedback is not necessary for cell-volume-dependence of histone mRNA concentrations

The observation that histone transcript concentrations decrease with $c \sim 1/V$ suggests that, similar to histone protein amounts (**Fig. 1e**), also histone transcript amounts are determined by gene copy number. We therefore measured the concentrations of representative histone transcripts in inducible-Whi5 diploids homozygous or hemizygous for *HTB2*. Again, we find that all histones analyzed exhibit a VDP close to -1 (**Supplementary Fig. 5a**), and as observed for Htb2 protein concentrations (**Fig. 1f**), the concentration of *HTB2* transcripts at a characteristic volume of 60 fL is clearly reduced in hemizygous compared to homozygous diploids (**Fig. 2e**). Moreover, we do not observe a significant overexpression of *HTB1* to compensate for the reduced *HTB2* transcript concentration (**Fig. 2e**).

bioRxiv preprint doi: https://doi.org/10.1101/2020.08.28.272492; this version posted August 29, 2020. The copyright holder for this preprint (which was not certified by peer review) is the author/funder, who has granted bioRxiv a license to display the preprint in perpetuity. It is made available under aCC-BY-NC-ND 4.0 International license.

So far, we have shown that in diploid cells with only one *HTB2* allele, the concentrations of *HTB2* transcript and protein are reduced compared to wild-type diploid cells. This highlights the absence of direct feedback mechanisms sensing and controlling the concentration of Htb2 with cell volume. However, extensive previous studies have shown that the eight budding yeast core histone genes show remarkably different modes of regulation. Specifically, only the gene pair *HTA1-HTB1* is known to exhibit dosage compensation, which is absent for *HTA2-HTB2*[20–22]. Moreover, three out of four core histone gene pairs, not including *HTA2-HTB2*, show negative feedback regulation of transcript concentration upon replication stress[14,28]. This feedback regulation is thought to be mediated by the HIR complex and to be dependent on *HIR1* and *RTT106*[29–31]. Thus, to test if HIR-dependent sensing and feedback regulation of histone transcript concentration may also be responsible for the cell-volume-dependence of HIR-regulated histone genes, we measured the cell-volume-dependence of representative histone genes (*HTB1*, *HTB2*, *HHF1*, *HHO1*) in *hir1*Δ and *rtt106*Δ strains. Strikingly, we find that neither Hir1 nor Rtt106 are needed for the decrease of concentration with cell volume for any of the tested histone transcripts (**Fig. 2f**, **Supplementary Fig. 5b**).

3'-to-5'-degradation by the nuclear exosome is not necessary for cell-volume-dependence of histone mRNA concentrations

The fact that the correct dependence of histone transcript concentration on cell volume does not require direct feedback suggests that instead it is an intrinsic property of either transcription rate or mRNA degradation. To test if degradation from the 3'-end by the nuclear exosome is required, we analyzed the cell-volume-dependence of histone transcript concentrations in strains where we deleted *RRP6*, a component of the nuclear exosome exonuclease[32,33]. As shown in **Fig. 2g**, we find that also in *rrp6*Δ cells, histone transcript concentrations decrease with cell volume. Interestingly, due to increased transcript concentrations in small cells (**Fig. 2h**, **Supplementary Fig. 5c**), this decrease with a VDP close to -2 is significantly stronger than in wild-type cells, suggesting that the volume-

bioRxiv preprint doi: https://doi.org/10.1101/2020.08.28.272492; this version posted August 29, 2020. The copyright holder for this preprint (which was not certified by peer review) is the author/funder, who has granted bioRxiv a license to display the preprint in perpetuity. It is made available under aCC-BY-NC-ND 4.0 International license.

dependence of histone transcripts is modulated by Rrp6-dependent degradation. Thus, while degradation by the nuclear exosome is not needed for the volume-dependent decrease of histone transcript concentrations, it may contribute to achieve the correct VDP of -1.

Histone promoters are sufficient for cell-volume-dependence of transcript concentrations

Given that degradation from the 3'-end does not seem to be crucial for the cell-volume-dependent decrease of histone transcript concentration, we next asked whether the promoter alone is sufficient to establish this cell-volume-dependence. To address this, we created strains that carry additional copies of either the *ACT1* or the histone *HHF1* promoter driving expression of the fluorescent protein mCitrine, regulated by the identical *ADH1* terminator (**Fig. 3a**). Strikingly, we find that the dependence of *mCitrine* transcript concentration on cell volume is determined by the promoter: If driven by the *ACT1* promoter, the VDP of *mCitrine* resembles that of endogenous *ACT1*; if driven by the *HHF1* promoter, it resembles that of endogenous *HHF1* (**Fig. 3b**).

To test if this also holds true for other histone promoters, we made use of the fact that the fluorescent reporter mCitrine enables a faster experimental readout using flow cytometry (**Fig. 3a**). First, we analyzed the cell-volume-dependent fluorescence of mCitrine expressed from the *ACT1* or *HHF1* promoters, which revealed that flow cytometry can be used to qualitatively distinguish the distinct volume-dependences. Similarly, we find that also all other histone promoters tested show significantly negative VDPs in haploid and diploid cells (**Fig. 3c – e, Supplementary Fig. 6**).

Histones not only need to be maintained at cell-volume-independent amounts, leading to a decrease of concentration with $1/V$, but also need to increase in proportion to cell ploidy (**Fig. 1**). This is in contrast to most other genes, which are maintained at a ploidy-independent concentration[34]. To test if the histone promoters are also sufficient to establish this distinct ploidy-dependence, we compared the expression level of the single *mCitrine* copy in diploid versus haploid cells. For *ACT1*, which needs to be maintained at a ploidy-independent concentration, we expect that a single gene allele in a

bioRxiv preprint doi: https://doi.org/10.1101/2020.08.28.272492; this version posted August 29, 2020. The copyright holder for this preprint (which was not certified by peer review) is the author/funder, who has granted bioRxiv a license to display the preprint in perpetuity. It is made available under aCC-BY-NC-ND 4.0 International license.

diploid should produce half of the protein compared to a homozygous diploid or haploid of similar volume[2]. Indeed, for the *ACT1* promoter we find that at a given cell volume, the concentration of mCitrine expressed from a single additional promoter is 50% lower in diploids compared to haploids (**Fig. 3d & f**). In contrast, for each of the three histone promoters tested, we observe that the concentration in diploids is considerably higher than 50% of that in haploids of comparable volume, with a ratio close to 1 for the *HTB1* promoter (**Fig. 3e & f, Supplementary Fig. 6**). This demonstrates that in addition to setting the cell-volume-dependent decrease in concentration, regulation by the histone promoters also largely accounts for the fact that histones are needed in proportion to ploidy.

Different cell-volume and ploidy dependences can be explained by competition of promoters for limiting transcriptional machinery

To better understand how the transcription rate of one specific promoter depends on cell volume and ploidy context, we sought to build a minimal model (**Fig. 4a**). Briefly, we considered two classes of promoters, a specific promoter of interest, p, present as a single copy, and a general pool of promoters, g, which are present as $n_h = 6000$ in haploids or $n_d = 12000$ copies in diploids. We then assume that transcription can be described by a single component of the transcriptional machinery, whose concentration c_{TM} stays constant with cell volume. Each promoter is competing for the transcriptional machinery, and is modelled as a single binding site for the limiting machinery component. Initiation, *i.e.* binding of the limiting machinery, occurs at a rate k_{on}^{p} or k_{on}^{g}, respectively. Furthermore, we assume that all other steps of transcription can be summarized in a single rate-limiting step, occurring at a rate k_{off}^{p} or k_{off}^{g}, respectively. Each transcript is then degraded with the same rate $k_{deg} = 1$. Depending on the parameters chosen for the specific promoter, the model predicts qualitatively different dependences of transcript concentration on cell-volume and ploidy (**Fig. 4b & c**). For example, at a given k_{off}^{p}, a high on-rate k_{on}^{p} can result in

bioRxiv preprint doi: https://doi.org/10.1101/2020.08.28.272492; this version posted August 29, 2020. The copyright holder for this preprint (which was not certified by peer review) is the author/funder, who has granted bioRxiv a license to display the preprint in perpetuity. It is made available under aCC-BY-NC-ND 4.0 International license.

histone-promoter-like behavior, *i.e.* cell volume-dependent but ploidy-independent transcript concentration. In contrast, at lower k_{on}^{p} we observe actin-promoter-like behavior, *i.e.* cell volume-independent but ploidy-dependent transcript concentration. Interestingly, due to the competition with general promoters, the transcript concentration can even increase with cell volume if k_{on}^{p} is much smaller than k_{on}^{g}.

One key prediction of this model is that if all other parameters are fixed, reducing k_{on}^{p} for a histone-like promoter should eventually shift its behavior to that of an actin-like promoter (**Fig. 4d**). To experimentally test this prediction, we aimed to decrease the initiation rate k_{on}^{p} of the *HHF1* and *HTB1* promoters by creating series of haploid and diploid strains with increasingly shorter fragments of the promoters, each truncated from the 5'-end (**Fig 5a**). Again, we used flow cytometry to analyze mCitrine expression driven by these additional, endogenously integrated promoter fragments. For both promoters we observe a decrease of mCitrine expression once part of the known upstream activating sequences (UASs)[35] are truncated (**Fig 5b, Supplementary Fig. 7a**). Fully consistent with the model, for both promoters, and for haploids and diploids, this drop in expression coincides with a change of the VDP towards 0 (**Fig 5b & c, Supplementary Fig. 7b & c**). At the same time and also consistent with the model, the ratio of the mCitrine concentration at a given volume in diploid compared to haploid cells decreases from close to 1 towards 0.5 (**Fig. 5c**). Thus, our analysis shows that for both the *HHF1* and *HTB1* promoter truncation series, a transition from histone-like to actin-like behavior occurs between the 450 bp to 300 bp truncations.

While we consistently observe the same qualitative trend in flow cytometry measurements, we note that the exact VDP depends on the forward scatter settings, which determine the observed cell-volume range. Thus, to quantitatively confirm our results, we repeated the experiment for the 450 bp and 300 bp truncations of the *HTB1* promoter using RT-qPCR. Again, we observe a change in the VDP towards 0, and a decrease of the ratio of the mCitrine concentration between diploid and

bioRxiv preprint doi: https://doi.org/10.1101/2020.08.28.272492; this version posted August 29, 2020. The copyright holder for this preprint (which was not certified by peer review) is the author/funder, who has granted bioRxiv a license to display the preprint in perpetuity. It is made available under aCC-BY-NC-ND 4.0 International license.

haploid cells from close to 1 to close to 0.5 (**Fig. 5d**). In summary, our analysis of the histone promoter truncations demonstrates that decreasing promoter strength can shift the volume- and ploidy-dependence of the histone promoters to an actin-like behavior, as predicted by our minimal model.

Discussion

Taken together, we identified a mechanism that allows cells to deal with a fundamental challenge – how to quantitatively couple histone production to DNA content even though total biosynthetic capacity is linked to cell volume instead. We found that this coordination is already achieved at the transcript level. While mRNA degradation and feedback mechanisms contribute to histone homeostasis, we find that competition for potentially limiting transcriptional machinery is sufficient to achieve differential regulation of histone and other transcript concentrations with cell volume and ploidy. Specifically, if transcription is limited by the availability of limiting machinery, larger cells with more machinery will produce proportionally more mRNA, maintaining constant transcript concentrations, which do not depend on ploidy. If transcription is instead limited by the gene itself, transcript concentrations will decrease with cell volume but will be proportional to ploidy. In addition to histones, other proteins will require differential regulation. For example, the G1/S inhibitors Whi5 in yeast[18] and Rb in mammalian cells[36] have recently been shown to decrease in concentration with cell volume, enabling cells to sense and control their size. Along those lines, a recent study suggested that many cell cycle regulators show differential transcriptional regulation with cell volume[37]. The simplicity of template-limited transcription therefore suggests that it may be broadly employed across species to differentially regulate the concentrations of larger subsets of proteins, in particular to couple the amount of DNA binding proteins to DNA content. Moreover, in addition to the ideal template- or machinery-limited regimes, cells can achieve a large variety of cell volume- and ploidy-dependences, which importantly can be decoupled from the expression level of a given gene by independently tuning its initiation and elongation rates. Specific regulation of mRNA

bioRxiv preprint doi: https://doi.org/10.1101/2020.08.28.272492; this version posted August 29, 2020. The copyright holder for this preprint (which was not certified by peer review) is the author/funder, who has granted bioRxiv a license to display the preprint in perpetuity. It is made available under aCC-BY-NC-ND 4.0 International license.

and protein degradation provides yet another level of control that cells can employ to tune the dependence of protein concentrations on cell volume and ploidy. In fact, our observation that the cell-volume-dependence of histone transcripts is even stronger in *rrp6* deletion cells, suggests that such additional regulation contributes to cell-volume-dependent histone homeostasis in budding yeast. To quantitatively understand the cell volume- and ploidy-dependence of protein homeostasis on a genome wide level, it will therefore be crucial to identify the rate-limiting steps of transcription and mRNA degradation as well as the corresponding rate-limiting molecules.

Materials and methods

Yeast strains

All yeast strains used in this work are based on W303 and were constructed using standard methods. Full genotypes of all strains are listed in **Supplementary Table 1.**

Inducible-Whi5 strain

In order to increase the range of observable cell volumes, we used strains with β-estradiol inducible *WHI5*, similarly described in previous works[18,38]. For this purpose, we deleted the endogenous alleles of the G1/S inhibitor *WHI5* and integrated one copy of *WHI5* expressed from an artificial, β-estradiol-inducible promoter system[19]. Specifically, this inducible promoter system consists of a β-estradiol-dependent, artificial transcription factor, which can bind an artificial promoter. This promoter is then used to induce *WHI5* expression.

To ensure that β-estradiol addition itself has no effect on cell growth, we grew cell cultures of a non-inducible *WHI5* haploid strain and cell cultures of a *whi5Δ* haploid strain, containing the β-estradiol-dependent, artificial transcription factor, but no copy of *WHI5*. We then added β-estradiol to those cultures and quantified the mean cell volumes after 24 h of growth in the presence of β-estradiol, by measuring the cell volume distributions using a Coulter Counter (Beckman Coulter, Z2 Particle Counter). Finally, we compared the mean cell volumes to the mean cell volumes obtained from cell

bioRxiv preprint doi: https://doi.org/10.1101/2020.08.28.272492; this version posted August 29, 2020. The copyright holder for this preprint (which was not certified by peer review) is the author/funder, who has granted bioRxiv a license to display the preprint in perpetuity. It is made available under aCC-BY-NC-ND 4.0 International license.

populations without β-estradiol addition (**Supplementary Fig. 3a**). In addition, we performed reverse-transcription-qPCR (RT-qPCR) on cell populations with and without β-estradiol addition and compared the obtained mean values for several genes (**Supplementary Fig. 3b & c**). For the non-inducible *WHI5* haploid strain, we could not identify a significant deviation of the population means between the cell populations with and without β-estradiol addition. For the *whi5Δ* haploid strain, containing only the β-estradiol-dependent, artificial transcription factor, we observed a slight but significant reduction of the relative mean mRNA concentrations of *HTA2, HHF2* and *HHO1* at 30 nM compared to 0 nM β-estradiol, which was consistent with a slightly increased mean cell volumes at 30 nM β-estradiol. In contrast, performing the same experimental procedure on cell cultures of an inducible *WHI5* haploid strain, leads to much stronger changes of mean cell volumes and relative mean mRNA concentrations for all histone genes, demonstrating that the observed decrease of histone mRNA concentrations is specific to the Whi5-dependent cell volume increase (**Supplementary Fig. 3a & d**). Significances were tested using two-tailed two-sample t-tests, after checking for normal distribution and equal variance distributions using a Shapiro-Wilk test and a Bartlett test, respectively.

Live-cell fluorescence microscopy

Cultures (3 mL) were grown at 30℃ in synthetic complete media containing 2% glycerol and 1% ethanol (SCGE) for at least 6 h in a shaking incubator at 250 rpm (Infors, Ecotron). Appropriate β-estradiol concentrations were then added to inducible cells (0 nM and 30 nM for haploids or 50 nM for diploids) and the cultures grown for at least 24 h to ensure steady-state conditions. Optical densities were measured using a spectrophotometer (Perkin Elmer, Lambda Bio+) and $OD_{600} < 1.0$ was maintained through appropriate dilutions during culture growth. For imaging, 1 mL of cells ($OD_{600} < 1.0$) was spun down at 10k g-force for 1 min (Thermo Fisher Scientific, Pico 17), resuspended in 200 µL SCGE and sonicated for 5 s (Bandelin electronics, HD2070 & UW2070).

bioRxiv preprint doi: https://doi.org/10.1101/2020.08.28.272492; this version posted August 29, 2020. The copyright holder for this preprint (which was not certified by peer review) is the author/funder, who has granted bioRxiv a license to display the preprint in perpetuity. It is made available under aCC-BY-NC-ND 4.0 International license.

100 µL of this cell suspension was then introduced in a Cellasic microfluidics Y04C (haploids and non-induced diploids) or Y04D (induced diploids) plate.

Live-cell fluorescence microscopy experiments were performed on a Zeiss LSM 800 microscope with additional epifluorescence setup using a Cellasic microfluidics device to ensure constant media (SCGE) flow in the microfluidics plate throughout the experiment. Experiments ran for 12 h with images being taken every 3 min using an automated stage (WSB Piezo Drive Can), a plan-apochromat 40x/1.3 oil immersion objective and an axiocam 506 camera. Phase-contrast images were taken at an illumination voltage of 4.5 V and an exposure time of 30 ms. *mCitrine* images were taken using the Colibri 511 LED module at 25% power and an exposure time of 10 ms. For each condition, at least two independent biological replicates were measured on different days.

To correct for inaccuracies of the x-y-stage between time points, movies were first aligned using a custom Fiji script. Then, cell segmentation and quantification of the fluorescent signal as well as subtraction of background fluorescence and cell-volume-dependent autofluorescence (determined from control strains not expressing a fluorescent protein), and determination of time points of cell birth, bud emergence, and cytokinesis were performed with MATLAB 2017b using previously described methods[17,18,39]. For our analyses, we only included cells born during the experiment. Total fluorescence intensity after background- and autofluorescence correction was used as a proxy for total protein amount.

In order to determine total protein concentrations as total protein amounts divided by cell volume, we calculated cell volumes based on phase-contrast images. Briefly, after segmentation, cell areas where aligned along their major axis. We then divided the cells into slices perpendicular to their major axis, each 1 pixel in width. To estimate cell volume, we then assumed rotational symmetry of each slice around its middle axis parallel to the cell's major axis, and summed the volumes of each slice to

bioRxiv preprint doi: https://doi.org/10.1101/2020.08.28.272492; this version posted August 29, 2020. The copyright holder for this preprint (which was not certified by peer review) is the author/funder, who has granted bioRxiv a license to display the preprint in perpetuity. It is made available under aCC-BY-NC-ND 4.0 International license.

obtain total cell volume. This allowed us to analyze protein amounts and protein concentrations as a function of cell volume.

Estimation of cell cycle phases and histone production period using live-cell microscopy

To test whether the decrease of histone concentrations with cell volume could be explained by a decrease in the S-phase duration, and thus a shorter time period during which histones are produced, we aimed to estimate the duration of the *histone production period* (H-period) from the Htb2-mCitrine fluorescent intensity traces. For each single cell, we first performed a constant linear fit in each of the two plateaus of the fluorescence intensity, linked to G1- or G2/M-phase, respectively, and denoted them as P_1 and P_2. P_1 was obtained by performing the linear fit through the data points of the fluorescent intensity trace from cell birth to first bud emergence, P_2 was obtained by performing the linear fit through the last 30 minutes of the fluorescent intensity trace. We then set a threshold of 5%, determined the last time point for which $I_{Htb2-mCitrine} < P_1 + 0.05 \cdot P_1$, and defined this time point as the beginning of the H-period. Similarly, we defined the first time point for which $I_{Htb2-mCitrine} > P_2 - 0.05 \cdot P_2$ as the end of the H-period. Finally, the duration of the H-period was calculated as the difference between those two time points. We defined G1-phase duration as the time from cell birth to first bud emergence, and G2/M duration as the time between the end of the H-period and cytokinesis.

RNA extraction and RT-qPCR

Cultures (25 mL) were grown at 30℃ in yeast peptone media containing 2% glucose (YPD) for at least 6 h in a shaking incubator at 250 rpm, before being washed and transferred to SCGE. The cultures were grown for at least 16 h before appropriate β-estradiol concentrations were added to inducible cells (0 nM, 10 nM and 30 nM). The cultures (final volume of 50 mL) were then grown for at least 24 h in order to ensure steady-state conditions. During culture growth, $OD_{600} < 1.0$ was

bioRxiv preprint doi: https://doi.org/10.1101/2020.08.28.272492; this version posted August 29, 2020. The copyright holder for this preprint (which was not certified by peer review) is the author/funder, who has granted bioRxiv a license to display the preprint in perpetuity. It is made available under aCC-BY-NC-ND 4.0 International license.

maintained through appropriate dilutions. Cell volume distributions of the cultures were measured with a Coulter counter after sonication for 5 s.

Remaining cell cultures were spun down at 4000 rpm for 5 min and the cell pellet resuspended in 50 µL nuclease-free water (Qiagen). Total RNA was extracted using a hot acidic phenol (Sigma-Aldrich) and chloroform (Thermo Fisher Scientific) extraction method adapted from an established protocol[40]. Yield of RNA was increased by precipitation in 100% ethanol (Merck Millipore) at -20℃ overnight, followed by a second precipitation in 100% ethanol at -80℃ for 2-4 h. As a quality check for total RNA extraction, agarose gel electrophoresis (1% agarose gel, run 30 min at 100 V) was performed to check for the presence of the 25s, 18s and 5.8s ribosomal RNA bands. Concentration and purity of the RNA samples were measured with a spectrophotometer (Thermo Fisher Scientific, NanoDrop 2000) at 260 nm and 280 nm. cDNA was then obtained from 800 ng total RNA in a PCR cycler (Applied Biosystems, ProFlex PCR system 3x32-well) using random primers and a high-capacity cDNA reverse transcription kit following the included protocol (Thermo Fisher Scientific).

Quantitative PCR (qPCR) measurements were carried out on a LightCycler 480 Multiwell Plate 96 (Roche) using a DNA-binding fluorescent dye (BioRad, SsoAdvanced Universal SYBR Green Supermix) and mRNA sequence specific primers (Sigma-Aldrich). The qPCR was performed with 2 µL of a 1:10 dilution of the cDNA for the genes *ACT1*, *HHO1*, *HTB2* and *mCitrine*, or a 1:100 dilution for all other genes. Melting curve data were analyzed to verify primer specificity. Each sample was measured in technical duplicates and the mean value C_P^{Gene} was used for further analyses if $\sigma_{C_P^{Gene}} < 0.5$. Relative concentrations, normalized on the reference gene *RDN18* were calculated using the equation:

$$log_2(relative\ concentration) = -(C_P^{Gene} - C_P^{RDN18})\#(1)$$

In order to analyze relative concentrations as a function of cell volume, the mean cell volumes were determined from the measured cell volume distributions.

bioRxiv preprint doi: https://doi.org/10.1101/2020.08.28.272492; this version posted August 29, 2020. The copyright holder for this preprint (which was not certified by peer review) is the author/funder, who has granted bioRxiv a license to display the preprint in perpetuity. It is made available under aCC-BY-NC-ND 4.0 International license.

Test for qPCR primer specificity

To test the specificity of the qPCR primer used to quantify histone mRNA concentrations, we analyzed deletion strains, where possible, for their respective deleted gene to check for unspecific primer binding. For example, we performed a qPCR measurement with the *HHO1* primers on a *hho1Δ* strain and compared the obtained C_p values with the C_p values obtained in the reference strain MS63-1 (**Supplementary Table 1**). We constructed deletion strains for the genes *HHO1*, *HTB2*, *HHF1*, *HHF2*, *HHT1* and *HHT2*, for which we obtained viable colonies without dramatic growth defects. RNA was extracted as described above, and 1 µg of total RNA was reverse-transcribed using the above mentioned high capacity cDNA synthesis kit. The qPCR was performed with 2 µL of a 1:10 dilution of each cDNA sample, and measured in 3 or 6 technical replicates. C_p values and melting curve data were analyzed to verify primer specificity. Results are shown in **Supplementary Table 2**, deletion strains used are listed in **Supplementary Table 1**, a list of all qPCR primers used can be found in **Supplementary Table 3.**

Flow Cytometry

Cultures (2 mL – 5 mL) were grown in YPD for at least 6 h in a shaking incubator (30℃, 250 rpm) before being washed and transferred to SCGE and grown for at least 16 h. Appropriate β-estradiol concentrations were then added to inducible cells (0 nM and 30 nM for haploids or 50 nM for diploids), and the cultures grown for at least 24 h in a final volume of 3 mL – 5 mL. During cell growth, $OD_{600} < 1.3$ was maintained through appropriate dilutions.

Cell volume distributions of cultures were measured with a Coulter counter after sonication for 5 s. Cells were fixed using a 37% formaldehyde solution (Sigma-Aldrich) by pipetting 100 µL of formaldehyde into 900 µL of cell cultures in order to achieve a final formaldehyde concentration of 3.7%. Cultures were incubated at room temperature on a rotator (VWR International, Tube Rotator) for 15 min, spun down at 10k g-force for 3 min and subsequently washed and resuspended in 100 µL

bioRxiv preprint doi: https://doi.org/10.1101/2020.08.28.272492; this version posted August 29, 2020. The copyright holder for this preprint (which was not certified by peer review) is the author/funder, who has granted bioRxiv a license to display the preprint in perpetuity. It is made available under aCC-BY-NC-ND 4.0 International license.

- 1000 µL 100mM potassium phosphate (pH 7.5). Samples were then stored on ice until being used for flow cytometry.

Flow Cytometry measurements were carried out on a benchtop flow cytometer with octagon and trigon detector arrays (BD Biosciences, LSR II). Strains expressing the fluorescent protein *mCitrine* were excited with a 488 nm coherent sapphire solid-state laser paired with a 530/30 nm filter set. Side-scatter voltage was set to 220 V for all measurements, voltages for forward-scatter and photomultiplier tubes were adjusted depending on whether haploid or diploid cells or both were being measured. However, identical settings were used for replicate experiments. After removing obvious outliers or potential doublets through standard gating strategies, at least 10.000 cells were imaged in the final stopping gate. For each experiment, cells not expressing *mCitrine* were measured to determine the cell-volume-dependent autofluorescence background which was subtracted from the mean fluorescence intensity of each sample measured in the same experiment. In order to calculate fluorescence concentrations, mean cell volumes were determined from the cell volume distributions measured with the Coulter counter. Mean fluorescence concentrations were then calculated by dividing the mean fluorescence intensity of each sample by its mean cell volume, allowing us to analyze mCitrine fluorescence concentrations as a function of cell volume.

Cell cycle analysis using flow cytometry

To get insights into the distributions of cell cycle phases in cell populations of non-inducible and inducible *WHI5* haploid and diploid strains, we performed cell cycle analysis using flow cytometry. For this purpose, cell cultures (5 mL) were grown in YPD for at least 6 h in a shaking incubator (30°C, 250 rpm), before being washed and transferred to SCGE; where appropriate β-estradiol concentrations were added (10 nM or 30 nM for haploid cells, 50 nM for diploid cells). The cultures were then grown for at least 24 h, assuring $OD_{600} < 1.3$ during culture growth through appropriate dilutions. Cell volume distributions of cultures were measured with a Coulter counter after sonication

bioRxiv preprint doi: https://doi.org/10.1101/2020.08.28.272492; this version posted August 29, 2020. The copyright holder for this preprint (which was not certified by peer review) is the author/funder, who has granted bioRxiv a license to display the preprint in perpetuity. It is made available under aCC-BY-NC-ND 4.0 International license.

for 5 s. To fixate the cells and subsequently stain the DNA, we followed an already established protocol[41]. Specifically, 1 mL of each cell culture was pipetted into 9 mL of cold 80% ethanol and incubated at 4℃ on a rotator overnight. The cultures were then spun down at 4000 rpm for 2 min and washed twice in 50 mM Tris-HCl (pH = 8.0). Cells were then successively treated with a 1 mg/mL RNase A (Thermo Fisher Scientific) solution for 40 min at 37℃, a 20 mg/mL Proteinase K (Promega) solution for 1 h at 37℃ and a 10x SYBR Green I (Sigma-Aldrich) solution for 1 h at room temperature. Between each treatment, cells were washed twice with 50 mM Tris-HCl and resuspended in 50 mM Tris-HCl. After the last treatment, cells were sonicated for 5 s. Flow Cytometry measurements were carried out on the benchtop flow cytometer described above, using the same laser, filter sets and side-scatter voltage. Settings for forward-scatter and photomultiplier tubes were adjusted depending on the condition measured. To estimate cell-cycle fractions, imaged DNA content frequency histograms were analyzed using Watson modelling. However, we noticed that for cell populations with large cell volumes (*i.e.* high β-estradiol concentrations), the DNA content distributions showed pronounced tails at large cell volumes that were not fit by the model. We speculate that this tail represents an increased mitochondrial DNA content in large cells[42], which suggests that a fraction of G1 cells would be wrongly identified as S phase. Thus, we decided to limit our analysis to classifying cells as either G1/S-phase or G2/M-phase (**Supplementary Fig. 1c**). Using this approach, we did not find a drastic influence of the β-estradiol concentration used for Whi5 induction on the cell cycle distributions.

Volume-dependence parameter

Analyzing protein and mRNA concentrations as a function of cell volume reveals a decrease of concentration with increasing cell volume for histones. In order to quantify this decrease, we performed a linear regression on the double logarithmic data and define the slope of the fit as the *volume-dependence parameter* (VDP):

bioRxiv preprint doi: https://doi.org/10.1101/2020.08.28.272492; this version posted August 29, 2020. The copyright holder for this preprint (which was not certified by peer review) is the author/funder, who has granted bioRxiv a license to display the preprint in perpetuity. It is made available under aCC-BY-NC-ND 4.0 International license.

$$log_2(c) = log_2(c_0) + \mathrm{VDP} \cdot log_2(V) \#(2)$$

459 The VDP gives us a quantitative measure for the relation of protein and mRNA concentrations with
460 cell volume: A negative VDP indicates a decrease of concentration with increasing cell volume. The
461 special case of $\mathrm{VDP} = -1$ corresponds to a decrease of concentration with $c \sim 1/V$, and therefore
462 signifies a constant amount of protein or mRNA with increasing cell volume. A positive VDP
463 indicates an increase of concentration with increasing cell volume, and $\mathrm{VDP} = 0$ corresponds to a
464 constant concentration c_0.

465 **Statistical analyses**

466 *Significance of VDPs*

467 To test for a significant deviation of the VDP from 0, we performed two-tailed one-sample t-tests on
468 the regression coefficients of the linear fit at a confidence level of $\alpha = 0.05$. Our null hypothesis H_0
469 assumes the respective coefficient to be equal to 0. In order to test for the significance of the VDP,
470 we are interested in the slope of the linear fit: for a p-value smaller than α, we reject H_0 and consider
471 the slope, *i.e.* the VDP, to be significantly different from 0.

472 To test whether the VDPs of two different conditions significantly deviate from each other, we used
473 a general linear regression model with a categorical variable, $Type$, to differentiate between the two
474 conditions analysed:

$$log_2(c) = log_2(c_0) + \mathrm{VDP}_0 \cdot log_2(V) + \delta_1 \cdot Type + \delta_2 \cdot Type \cdot log_2(V) \#(3)$$

475 with c_0 and VDP_0 corresponding to the reference condition ($Type = 0$), δ_1 describing the average
476 difference in the intercepts of the linear fits between the two conditions, and δ_2 describing the
477 change in the slopes (VDPs) between the two conditions. In order to test for a significant difference
478 between the two VDPs, we perform a two-tailed one-sample t-test on δ_2, with the null hypothesis H_0
479 assuming $\delta_2 = 0$, at a confidence level of $\alpha = 0.05$. For a p-value smaller than α, we reject H_0 and

bioRxiv preprint doi: https://doi.org/10.1101/2020.08.28.272492; this version posted August 29, 2020. The copyright holder for this preprint (which was not certified by peer review) is the author/funder, who has granted bioRxiv a license to display the preprint in perpetuity. It is made available under aCC-BY-NC-ND 4.0 International license.

consider the change between the two slopes to be significant, *i.e.* we consider the two VDPs to be significantly different from each other.

Error estimation of concentrations at 60 fL

To calculate concentrations at a characteristic cell volume of 60 fL with respective error estimates, we evaluated the linear fits to the double logarithmic data at 60 fL and estimated the 95 % confidence intervals of the fit at 60 fL. When normalizing the concentration to a chosen value x, errors were calculated using error propagation:

$$\Delta y = y \cdot \sqrt{\left(\frac{\Delta c^2}{c^2}\right)^2 + \left(\frac{\Delta x^2}{x^2}\right)^2} \quad \#(4)$$

with y being the new normalized concentration and c the previously calculated concentration.

To estimate the error associated with the ratio between the concentrations at 60 fL in haploids and diploids, we used bootstrap analysis. Specifically, we treated the measurements of protein or mRNA concentration and corresponding cell volume as a set of linked variables, both for haploid and diploid cells. We then resampled n = 10000 populations of same size by random sampling with replacement from this experimental two-dimensional population. Next, we performed a linear regression on the double logarithmic data for each of the resampled populations and estimated the concentration at 60 fL, giving us a distribution of n = 10000 concentrations at 60 fL for both haploid and diploid cells. Finally, we randomly selected a concentration in each of those distributions, and divide the concentration for diploids by the concentration for haploids. We repeated this process 10000 times with replacement to obtain a distribution of n = 10000 concentration ratios, for which we calculate the median and the 2.5- and 97.5-percentiles.

Minimal model

To obtain mechanistic insight on how the transcription rate of one specific promoter depends on cell

bioRxiv preprint doi: https://doi.org/10.1101/2020.08.28.272492; this version posted August 29, 2020. The copyright holder for this preprint (which was not certified by peer review) is the author/funder, who has granted bioRxiv a license to display the preprint in perpetuity. It is made available under aCC-BY-NC-ND 4.0 International license.

volume and ploidy context, we sought to build a minimal model. For this, we consider transcription being limited by one component of the transcriptional machinery, potentially a subunit of the RNA polymerase. In addition, we assume transcript degradation to be the same for all transcripts, and set the corresponding degradation rate $k_{deg} = 1$, *i.e.*, all other rates are normalized with respect to k_{deg}. Note that in the case of stable transcripts, k_{deg} also describes dilution of transcripts by cell growth.

To account for the competition of different promoters for a finite number of the limiting component of the transcriptional machinery (TM), our model distinguishes two classes of promoters - a *general pool* of promoters, g, with $n_h \approx 6000$ (haploids) or $n_d \approx 12000$ (diploids), and a single *promoter of interest*, p, present as a single copy. We describe each promoter as one single binding site for TM and denote the number of TM bound to general promoters as R^g. Binding of TM at the single promoter of interest is described by R^p, which can assume values between 0 (not bound) and 1 (bound). Moreover, R^f denotes the number of free TM. We assume that the total number of TM (free and bound) scales proportionally to cell volume V and is given by

$$R^g + R^p + R^f = c_{TM} V \#(5)$$

with c_{TM} being the total TM concentration.

Assuming that the arrival of TM at promoters is proportional to the concentration of free TM, the change in number of bound general promoters over time is given by following equation:

$$\frac{dR^g}{dt} = k_{on}^g \left(n_{h/d} - R^g\right) \frac{R^f}{V} - k_{off}^g R^g \#(6)$$

where k_{on}^g is the rate at which transcription is being initiated at each general promoter, $n_{h/d} - R^g$ are the number of general promoters not bound to TM in haploids or diploids, respectively, and k_{off}^g models the rate at which bound TM complete transcriptional elongation.

Similarly, the change in binding of *TM* to the single promoter of interest over time is given by:

bioRxiv preprint doi: https://doi.org/10.1101/2020.08.28.272492; this version posted August 29, 2020. The copyright holder for this preprint (which was not certified by peer review) is the author/funder, who has granted bioRxiv a license to display the preprint in perpetuity. It is made available under aCC-BY-NC-ND 4.0 International license.

$$\frac{dR^p}{dt} = k_{on}^p(1 - R^p)\frac{R^f}{V} - k_{off}^p R^p \#(7)$$

with parameters k_{on}^p and k_{off}^p representing transcriptional initiation and elongation, respectively, at the promoter of interest.

Solving (6) and (7) at steady-state ($\frac{dR^g}{dt} = \frac{dR^p}{dt} = 0$), constraints the number of bound TMs via the following nonlinear equations

$$k_{on}^g\left(n_{h/d} - R^g\right)\frac{R^f}{V} = k_{off}^g R^g \#(8)$$

$$k_{on}^p(1 - R^p)\frac{R^f}{V} = k_{off}^p R^p \#(9)$$

Finally, the steady-state concentration of transcripts produced from the single promoter of interest is equal to $k_{off}^p R^p/V$.

Given a set of parameters $c_{TM}, k_{on}^g, k_{off}^g, k_{on}^p\ k_{off}^p$, numerically solving equations (5), (8) and (9) allows to calculate the transcript concentration, generated by the single promoter of interest as a function of cell volume V. We set $c_{TM} = 2000, k_{on}^g = 1, k_{off}^g = k_{off}^p = 3$ and calculate the steady-state concentration in haploids and diploids over cell volume for $k_{on}^p = [0.01, 100]$.

In order to determine the VDP as a function of k_{on}^p, we calculated the concentration for each value of k_{on}^p over a cell volume range of $V = \left[\frac{1}{3}, 3\right]$ and performed a linear regression fit on the logarithm of the concentration as a function of the logarithm of the cell volume, with cell volumes being equally spaced on the log scale. The VDP is then determined as the slope of the linear fit.

Data availability statement

Yeast strains and raw data are available upon reasonable request.

bioRxiv preprint doi: https://doi.org/10.1101/2020.08.28.272492; this version posted August 29, 2020. The copyright holder for this preprint (which was not certified by peer review) is the author/funder, who has granted bioRxiv a license to display the preprint in perpetuity. It is made available under aCC-BY-NC-ND 4.0 International license.

Code availability statement

Additional information on image analysis approaches described in the methods and previous publications is available upon reasonable request.

References

1. Marguerat, S. & Bähler, J. Coordinating genome expression with cell size. *Trends Genet.* **28**, 560–565 (2012).

2. Schmoller, K. M. & Skotheim, J. M. The Biosynthetic Basis of Cell Size Control. *Trends Cell Biol.* **25**, 793–802 (2015).

3. Zhurinsky, J. *et al.* A coordinated global control over cellular transcription. *Curr. Biol.* **20**, 2010–2015 (2010).

4. Padovan-Merhar, O. *et al.* Single Mammalian Cells Compensate for Differences in Cellular Volume and DNA Copy Number through Independent Global Transcriptional Mechanisms. *Mol. Cell* **58**, 339–352 (2015).

5. Sun, X.-M. *et al.* Size-dependent increase in RNA Polymerase II initiation rates mediates gene expression scaling with cell size. *bioRxiv Mol. Biol.* (2019) doi:10.1101/754788.

6. Nadal-Ribelles, M. *et al.* Sensitive high-throughput single-cell RNA-seq reveals within-clonal transcript correlations in yeast populations. *Nat. Microbiol.* (2019) doi:10.1038/s41564-018-0346-9.

7. Amodeo, A. A., Jukam, D., Straight, A. F. & Skotheim, J. M. Histone titration against the genome sets the DNA-to-cytoplasm threshold for the Xenopus midblastula transition. *Proc. Natl. Acad. Sci. U. S. A.* (2015) doi:10.1073/pnas.1413990112.

8. Joseph, S. R. *et al.* Competition between histone and transcription factor binding regulates the

bioRxiv preprint doi: https://doi.org/10.1101/2020.08.28.272492; this version posted August 29, 2020. The copyright holder for this preprint (which was not certified by peer review) is the author/funder, who has granted bioRxiv a license to display the preprint in perpetuity. It is made available under aCC-BY-NC-ND 4.0 International license.

559 onset of transcription in zebrafish embryos. *Elife* (2017) doi:10.7554/eLife.23326.

560 9. Hauer, M. H. *et al.* Histone degradation in response to DNA damage enhances chromatin
561 dynamics and recombination rates. *Nat. Struct. Mol. Biol.* (2017) doi:10.1038/nsmb.3347.

562 10. Chari, S., Wilky, H., Govindan, J. & Amodeo, A. A. Histone concentration regulates the cell
563 cycle and transcription in early development. *Dev.* (2019) doi:10.1242/dev.177402.

564 11. Kim, U. J., Han, M., Kayne, P. & Grunstein, M. Effects of histone H4 depletion on the cell
565 cycle and transcription of Saccharomyces cerevisiae. *EMBO J.* (1988) doi:10.1002/j.1460-
566 2075.1988.tb03060.x.

567 12. Han, M., Chang, M., Kim, U. J. & Grunstein, M. Histone H2B repression causes cell-cycle-
568 specific arrest in yeast: Effects on chromosomal segregation, replication, and transcription.
569 *Cell* (1987) doi:10.1016/0092-8674(87)90237-6.

570 13. Meeks-Wagner, D. & Hartwell, L. H. Normal stoichiometry of histone dimer sets is necessary
571 for high fidelity of mitotic chromosome transmission. *Cell* **44**, 43–52 (1986).

572 14. Eriksson, P. R., Ganguli, D., Nagarajavel, V. & Clark, D. J. Regulation of histone gene
573 expression in budding yeast. *Genetics* **191**, 7–20 (2012).

574 15. Kurat, C. F. *et al.* Regulation of histone gene transcription in yeast. *Cell. Mol. Life Sci.* **71**,
575 599–613 (2014).

576 16. Gunjan, A. & Verreault, A. A Rad53 Kinase-Dependent Surveillance Mechanism that
577 Regulates Histone Protein Levels in S. cerevisiae. *Cell* **115**, 537–549 (2003).

578 17. Doncic, A., Eser, U., Atay, O. & Skotheim, J. M. An Algorithm to Automate Yeast
579 Segmentation and Tracking. *PLoS One* **8**, (2013).

580 18. Schmoller, K. M., Turner, J. J., Kõivomägi, M. & Skotheim, J. M. Dilution of the cell cycle

bioRxiv preprint doi: https://doi.org/10.1101/2020.08.28.272492; this version posted August 29, 2020. The copyright holder for this preprint (which was not certified by peer review) is the author/funder, who has granted bioRxiv a license to display the preprint in perpetuity. It is made available under aCC-BY-NC-ND 4.0 International license.

581 inhibitor Whi5 controls budding-yeast cell size. *Nature* **526**, 268–272 (2015).

582 19. Ottoz, D. S. M., Rudolf, F. & Stelling, J. Inducible, tightly regulated and growth condition-
583 independent transcription factor in Saccharomyces cerevisiae. *Nucleic Acids Res.* **42**, (2014).

584 20. Norris, D. & Osley, M. A. The two gene pairs encoding H2A and H2B play different roles in
585 the Saccharomyces cerevisiae life cycle. *Mol. Cell. Biol.* (1987) doi:10.1128/mcb.7.10.3473.

586 21. Moran, L., Norris, D. & Osley, M. A. A yeast H2A-H2B promoter can be regulated by
587 changes in histone gene copy number. *Genes Dev.* (1990) doi:10.1101/gad.4.5.752.

588 22. Cross, S. L. & Smith, M. M. Comparison of the structure and cell cycle expression of mRNAs
589 encoded by two histone H3-H4 loci in Saccharomyces cerevisiae. *Mol. Cell. Biol.* **8**, 945–54
590 (1988).

591 23. von der Haar, T. A quantitative estimation of the global translational activity in
592 logarithmically growing yeast cells. *BMC Syst. Biol.* (2008) doi:10.1186/1752-0509-2-87.

593 24. Williamson, D. H. & Scopes, A. W. The distribution of nucleic acids and protein between
594 different sized yeast cells. *Exp. Cell Res.* (1961) doi:10.1016/0014-4827(61)90258-0.

595 25. Mena, A. *et al.* Asymmetric cell division requires specific mechanisms for adjusting global
596 transcription. *Nucleic Acids Res.* **45**, 12401–12412 (2017).

597 26. Hereford, L., Fahrner, K., Woolford, J., Rosbash, M. & Kaback, D. B. Isolation of yeast
598 histone genes H2A and H2B. *Cell* (1979) doi:10.1016/0092-8674(79)90237-X.

599 27. Smith, M. M. & Murray, K. Yeast H3 and H4 histone messenger RNAs are transcribed from
600 two non-allelic gene sets. *J. Mol. Biol.* (1983) doi:10.1016/S0022-2836(83)80163-6.

601 28. Libuda, D. E. & Winston, F. Alterations in DNA replication and histone levels promote
602 histone gene amplification in Saccharomyces cerevisiae. *Genetics* (2010)

bioRxiv preprint doi: https://doi.org/10.1101/2020.08.28.272492; this version posted August 29, 2020. The copyright holder for this preprint (which was not certified by peer review) is the author/funder, who has granted bioRxiv a license to display the preprint in perpetuity. It is made available under aCC-BY-NC-ND 4.0 International license.

603 doi:10.1534/genetics.109.113662.

604 29. Fillingham, J. *et al.* Two-Color Cell Array Screen Reveals Interdependent Roles for Histone
605 Chaperones and a Chromatin Boundary Regulator in Histone Gene Repression. *Mol. Cell* **35**,
606 340–351 (2009).

607 30. Zunder, R. M. & Rine, J. Direct Interplay among Histones, Histone Chaperones, and a
608 Chromatin Boundary Protein in the Control of Histone Gene Expression. *Mol. Cell. Biol.* **32**,
609 4337–4349 (2012).

610 31. Feser, J. *et al.* Elevated Histone Expression Promotes Life Span Extension. *Mol. Cell* (2010)
611 doi:10.1016/j.molcel.2010.08.015.

612 32. Canavan, R. & Bond, U. Deletion of the nuclear exosome component RRP6 leads to continued
613 accumulation of the histone mRNA HTB1 in S-phase of the cell cycle in Saccharomyces
614 cerevisiae. *Nucleic Acids Res.* (2007) doi:10.1093/nar/gkm691.

615 33. Beggs, S., James, T. C. & Bond, U. The PolyA tail length of yeast histone mRNAs varies
616 during the cell cycle and is influenced by Sen1p and Rrp6p. *Nucleic Acids Res.* **40**, 2700–2711
617 (2012).

618 34. Wu, C. Y., Alexander Rolfe, P., Gifford, D. K. & Fink, G. R. Control of transcription by cell
619 size. *PLoS Biol.* **8**, (2010).

620 35. Osley, M. A., Gould, J., Kim, S., Kane, M. & Hereford, L. Identification of sequences in a
621 yeast histone promoter involved in periodic transcription. *Cell* **45**, 537–544 (1986).

622 36. Zatulovskiy, E., Berenson, D. F., Topacio, B. R. & Skotheim, J. M. overexpression increased
623 cell size in tissue culture and a mouse cancer model, while. (2018).

624 37. Chen, Y., Zhao, G., Zahumensky, J., Honey, S. & Futcher, B. Differential Scaling of Gene
625 Expression with Cell Size May Explain Size Control in Budding Yeast. *Mol. Cell* (2020)

bioRxiv preprint doi: https://doi.org/10.1101/2020.08.28.272492; this version posted August 29, 2020. The copyright holder for this preprint (which was not certified by peer review) is the author/funder, who has granted bioRxiv a license to display the preprint in perpetuity. It is made available under aCC-BY-NC-ND 4.0 International license.

626 doi:10.1016/j.molcel.2020.03.012.

627 38. Kukhtevich, I. V., Lohrberg, N., Padovani, F., Schneider, R. & Schmoller, K. M. Cell size sets
628 the diameter of the budding yeast contractile ring. *Nat. Commun.* (2020) doi:10.1038/s41467-
629 020-16764-x.

630 39. Chandler-Brown, D., Schmoller, K. M., Winetraub, Y. & Skotheim, J. M. The Adder
631 Phenomenon Emerges from Independent Control of Pre- and Post-Start Phases of the Budding
632 Yeast Cell Cycle. *Curr. Biol.* **27**, 2774-2783.e3 (2017).

633 40. Collart, M. A. & Oliviero, S. Preparation of Yeast RNA. *Curr. Protoc. Mol. Biol.* (1993)
634 doi:10.1002/0471142727.mb1312s23.

635 41. Örd, M., Venta, R., Möll, K., Valk, E. & Loog, M. Cyclin-Specific Docking Mechanisms
636 Reveal the Complexity of M-CDK Function in the Cell Cycle. *Mol. Cell* (2019)
637 doi:10.1016/j.molcel.2019.04.026.

638 42. Rafelski, S. M. *et al.* Mitochondrial network size scaling in budding yeast. *Science (80-.).*
639 (2012) doi:10.1126/science.1225720.

640

641

bioRxiv preprint doi: https://doi.org/10.1101/2020.08.28.272492; this version posted August 29, 2020. The copyright holder for this preprint (which was not certified by peer review) is the author/funder, who has granted bioRxiv a license to display the preprint in perpetuity. It is made available under aCC-BY-NC-ND 4.0 International license.

Acknowledgments

We thank Matthew Swaffer and Anika Seel for sharing strains, Thomas Hofer and Elfriede Nößner from the HMGU-Immunoanalytics-Core Facility for support with flow cytometry, and the Institute of Functional Epigenetics and the Skotheim lab for discussions. We thank Matthew Swaffer, Amanda Amodeo and Jan Skotheim for comments on the manuscript. This work was supported by the DFG through project SCHM3031/4-1, by the Human Frontier Science Program (career development award to K.M.S) as well as the AMPro program (ZT0026) and the Helmholtz Gesellschaft. A.S. was supported by NIH grants 5R01GM124446 and 5R01GM126557.

Competing interests

The authors declare no competing interests.

bioRxiv preprint doi: https://doi.org/10.1101/2020.08.28.272492; this version posted August 29, 2020. The copyright holder for this preprint (which was not certified by peer review) is the author/funder, who has granted bioRxiv a license to display the preprint in perpetuity. It is made available under aCC-BY-NC-ND 4.0 International license.

Figures

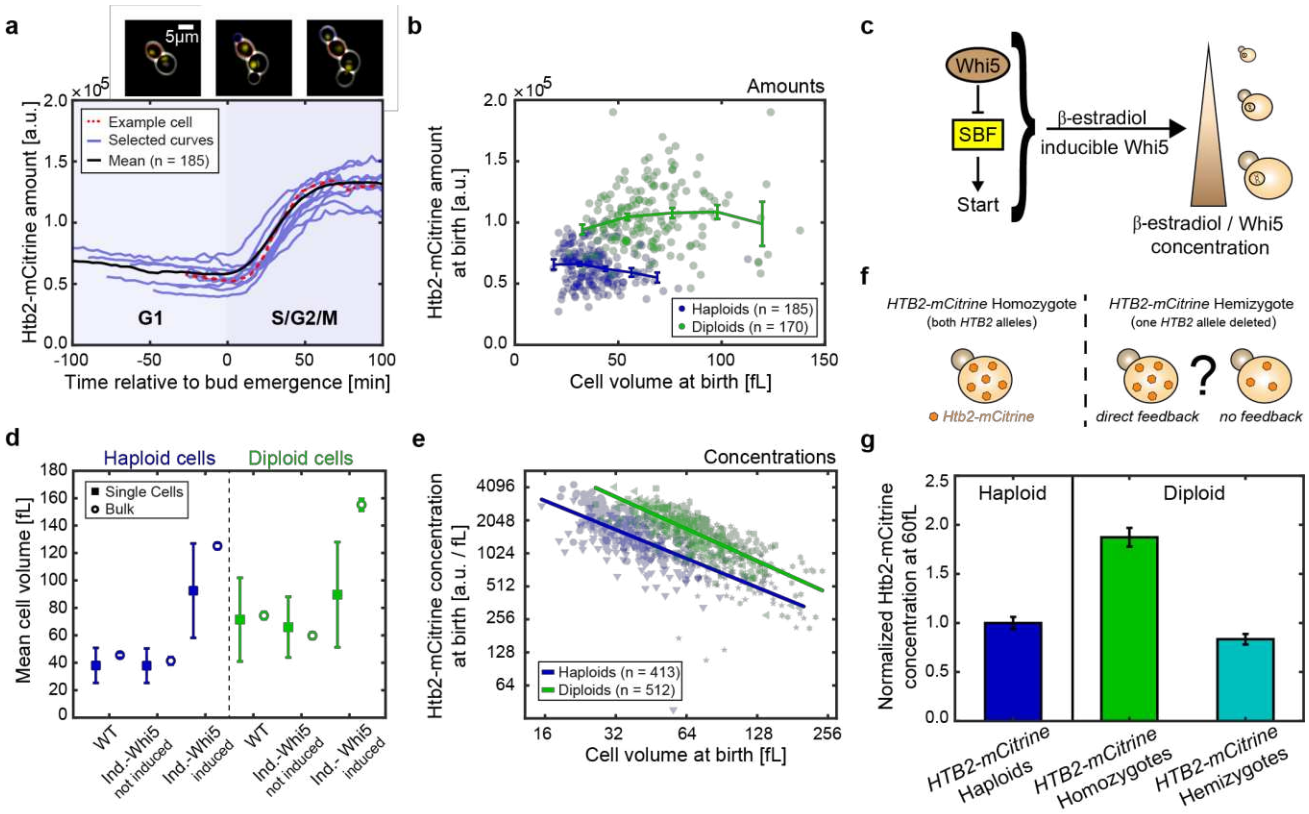

Figure 1. Htb2-mCitrine protein concentrations measured by live-cell fluorescence microscopy decrease with cell volume and increase with ploidy. (a) Htb2-mCitrine amounts during the first cell cycle of new-born cells. Red dashed trace highlights data corresponding to cells shown in the microscopy images (new-born cell: red outline, its bud: blue outline), blue traces show additional randomly selected example curves, black line the mean of n = 185 cells. All traces are aligned at the time of first bud emergence (t = 0). (b) Htb2-mCitrine amounts at birth for haploid (blue) and diploid (green) cells as a function of cell volume. Lines connect binned means, error bars indicate standard errors. (c) Whi5 controls cell volume in a dose-dependent manner. To manipulate cell volume, the endogenous allele is replaced by a copy of *WHI5* expressed from an artificial, β-estradiol-inducible promoter. Adding higher β-estradiol concentrations results in cells with bigger mean cell volumes. (d) Mean cell volumes for non-inducible (WT) and inducible haploids (blue) and diploids (green) measured in *HTB2-mCitrine* single cells with live-cell fluorescence microscopy (■), or in bulk populations of cells with untagged *HTB2* with a Coulter counter (○). Error bars indicate standard

bioRxiv preprint doi: https://doi.org/10.1101/2020.08.28.272492; this version posted August 29, 2020. The copyright holder for this preprint (which was not certified by peer review) is the author/funder, who has granted bioRxiv a license to display the preprint in perpetuity. It is made available under aCC-BY-NC-ND 4.0 International license.

683 deviations of the mean between single cells for single cell measurements
684 ($n_{haploid}^{WT} = 185$, $n_{haploid}^{not\ ind.} = 120$, $n_{haploid}^{ind.} = 108$, $n_{diploid}^{WT} = 170$, $n_{diploid.}^{not\ ind.} = 99$, $n_{diploid}^{ind} = 243$)
685 or the standard deviation of the population means across 5 biological replicates for bulk
686 measurements. Haploid cells were induced with 30 nM β-estradiol, diploid cells with 50 nM. Note
687 that no β-estradiol was used in the microfluidic device during the microscopy experiments, resulting
688 in a gradual decrease of cell volume of induced cells after the start of the experiment. (e) Htb2-
689 mCitrine concentrations of non-inducible and inducible haploids and diploids as a function of cell
690 volume are shown in a double logarithmic plot. Individual data points for the different conditions (▼
691 0 nM, ● WT, ★ 30 nM, for haploids and ◀ 0 nM, ■ WT, ✶ 50 nM, for diploids) are highlighted in
692 blue (haploids) and green (diploids). Lines show linear fits to the double logarithmic data. (f)
693 Illustration of the impact of potential feedback mechanisms on the concentration of Htb2-mCitrine
694 concentration in a *HTB2-mCitrine/htb2Δ* hemizygous diploid compared to a *HTB2-mCitrine*
695 homozygous diploid. (g) Htb2-mCitrine concentrations at 60 fL for haploids (blue), *HTB2-mCitrine*
696 homozygous diploids (green) and *HTB2-mCitrine/htb2Δ* hemizygous diploids (teal) normalized on
697 concentration at 60 fL in haploids. Error bars are derived by error propagation of the 95% confidence
698 interval of the linear fit at 60 fL.
699
700
701
702
703
704
705

bioRxiv preprint doi: https://doi.org/10.1101/2020.08.28.272492; this version posted August 29, 2020. The copyright holder for this preprint (which was not certified by peer review) is the author/funder, who has granted bioRxiv a license to display the preprint in perpetuity. It is made available under aCC-BY-NC-ND 4.0 International license.

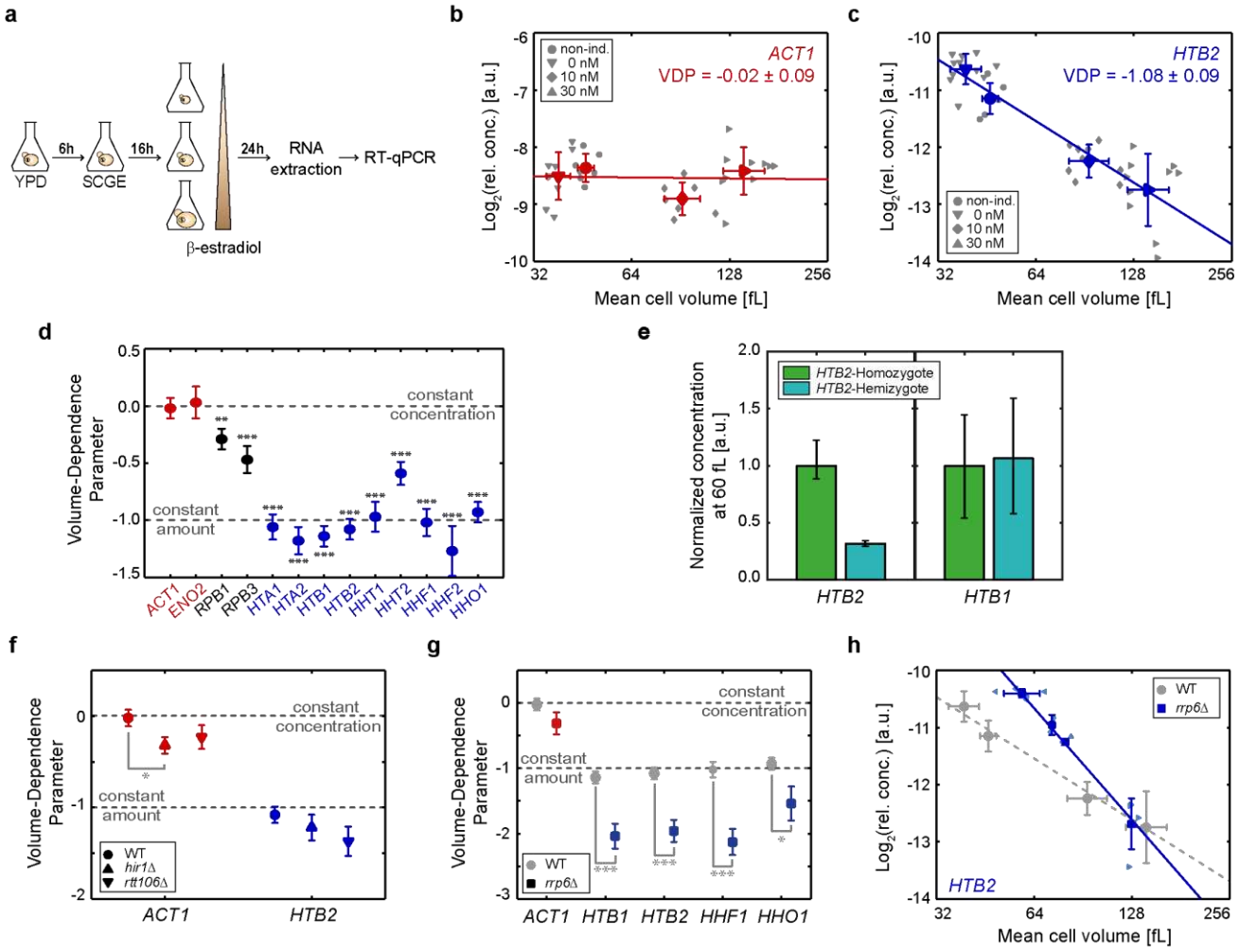

Figure 2. Histone mRNA concentrations decrease with cell volume and increase with ploidy. (a) Experimental procedure for RT-qPCR measurements. Cells were grown for at least 24 h at the respective β-estradiol concentration before extracting total RNA and performing RT-qPCR. (b & c) Relative *ACT1* (b) or *HTB2* (c) mRNA concentrations (normalized on *RDN18*) for non-inducible and inducible haploid cells over mean cell volume are shown in a double logarithmic plot. Individual data points for the different conditions (▼ 0 nM, ● non-inducible, ◆ 10 nM, ▲ 30 nM) are highlighted in grey. Red (b) or blue (c) symbols indicate the mean of the different conditions. Error bars indicate standard deviations for n ≥ 7 biological replicates. Lines show linear fits to the double logarithmic data, with volume-dependence parameters (VDPs) determined as the slope of the fit. (d) Summary of the VDPs for all measured genes. Error bars indicate the standard error of the slope;

bioRxiv preprint doi: https://doi.org/10.1101/2020.08.28.272492; this version posted August 29, 2020. The copyright holder for this preprint (which was not certified by peer review) is the author/funder, who has granted bioRxiv a license to display the preprint in perpetuity. It is made available under aCC-BY-NC-ND 4.0 International license.

718 significances that the VDP is different from 0: **p<0.01, ***p<0.001. (e) Median mRNA
719 concentrations at 60 fL of *HTB2* (left) and *HTB1* (right) in diploid *HTB2* homozygous (green) and
720 *HTB2/htb2*Δ hemizygous (teal) strains, normalized on the respective median concentration of the
721 *HTB2*-homozygote. Error bars indicate the 2.5- and 97.5-percentiles determined from 10000
722 bootstrap samples. (f & g) Summary of VDPs for *hir1*Δ and *rtt106*Δ (f) as well as *rrp6*Δ (g) deletion
723 strains. Error bars indicate the standard error. Significant VDP deviation from the wild-type VDP
724 (carrying no deletion) was tested using linear regressions; *p<0.05, ***p<0.001. (h) Relative *HTB2*
725 mRNA concentrations (normalized on *RDN18*) for inducible and non-inducible haploid cells over
726 mean cell volume, shown in a double logarithmic plot. Data corresponding to the *rrp6*Δ cells are
727 highlighted in blue. Light blue symbols highlight the different conditions (◆ non-inducible, ◄ 0 nM,
728 ▲ 10 nM, ► 30 nM). Dark blue symbols (■) indicate the mean for each condition. Grey symbols (●)
729 indicate the mean for each condition of the wild-type (carrying no deletion). Lines show the linear
730 fits to the double logarithmic data.

731

732

733

734

735

736

737

738

739

bioRxiv preprint doi: https://doi.org/10.1101/2020.08.28.272492; this version posted August 29, 2020. The copyright holder for this preprint (which was not certified by peer review) is the author/funder, who has granted bioRxiv a license to display the preprint in perpetuity. It is made available under aCC-BY-NC-ND 4.0 International license.

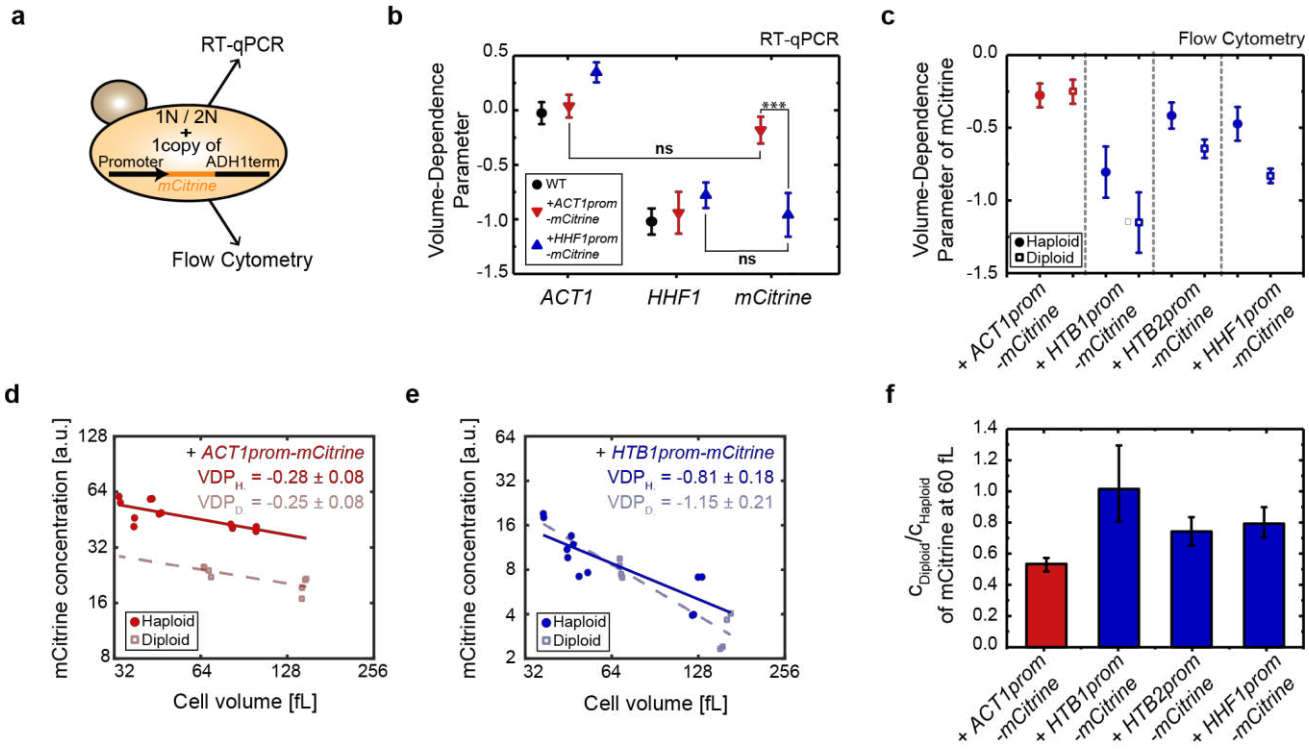

740

741 **Figure 3.** Histone promoters are sufficient for cell-volume- and ploidy-dependence of transcript
742 concentrations. (a) Illustration of haploid (1N) or diploid (2N) strains carrying a single additional
743 copy of a promoter of interest, driving the expression of the fluorescent reporter *mCitrine* regulated
744 by the *ADH1* terminator. RT-qPCR or flow cytometry were used to analyze expression of the
745 fluorescent reporter. (b) Summary of VDPs determined with RT-qPCR for the genes *ACT1*, *HHF1*
746 and *mCitrine* in a wild-type strain (black •), a strain carrying an additional *ACT1* promoter (red ▼),
747 or a strain carrying an additional *HHF1* promoter (blue ▲). Error bars indicate the standard error.
748 Significant VDP deviation between two genes was tested using linear regressions; ***p<0.001. (c)
749 Summary of VDPs determined with flow cytometry for different strains in haploid (●) and diploid
750 (□) cells. Error bars indicate the standard error. (d – e) *mCitrine* concentration, driven by an
751 additional copy of the *ACT1* (d) or *HTB1* (e) promoter in haploid (●) and diploid (□) cells, shown as
752 a function of cell volume in a double logarithmic plot. Lines show linear fits to the double
753 logarithmic data with volume-dependence parameters (VDPs) determined as the slope of the fit, with
754 respective standard error. (f) Median concentration of mCitrine in diploid cells compared to the

bioRxiv preprint doi: https://doi.org/10.1101/2020.08.28.272492; this version posted August 29, 2020. The copyright holder for this preprint (which was not certified by peer review) is the author/funder, who has granted bioRxiv a license to display the preprint in perpetuity. It is made available under aCC-BY-NC-ND 4.0 International license.

755 median concentration in haploid cells at 60 fL. Error bars indicate the 2.5- and 97.5-percentiles
756 determined from 10000 bootstrap samples.

757

758

759

760

761

762

763

764

765

766

767

bioRxiv preprint doi: https://doi.org/10.1101/2020.08.28.272492; this version posted August 29, 2020. The copyright holder for this preprint (which was not certified by peer review) is the author/funder, who has granted bioRxiv a license to display the preprint in perpetuity. It is made available under aCC-BY-NC-ND 4.0 International license.

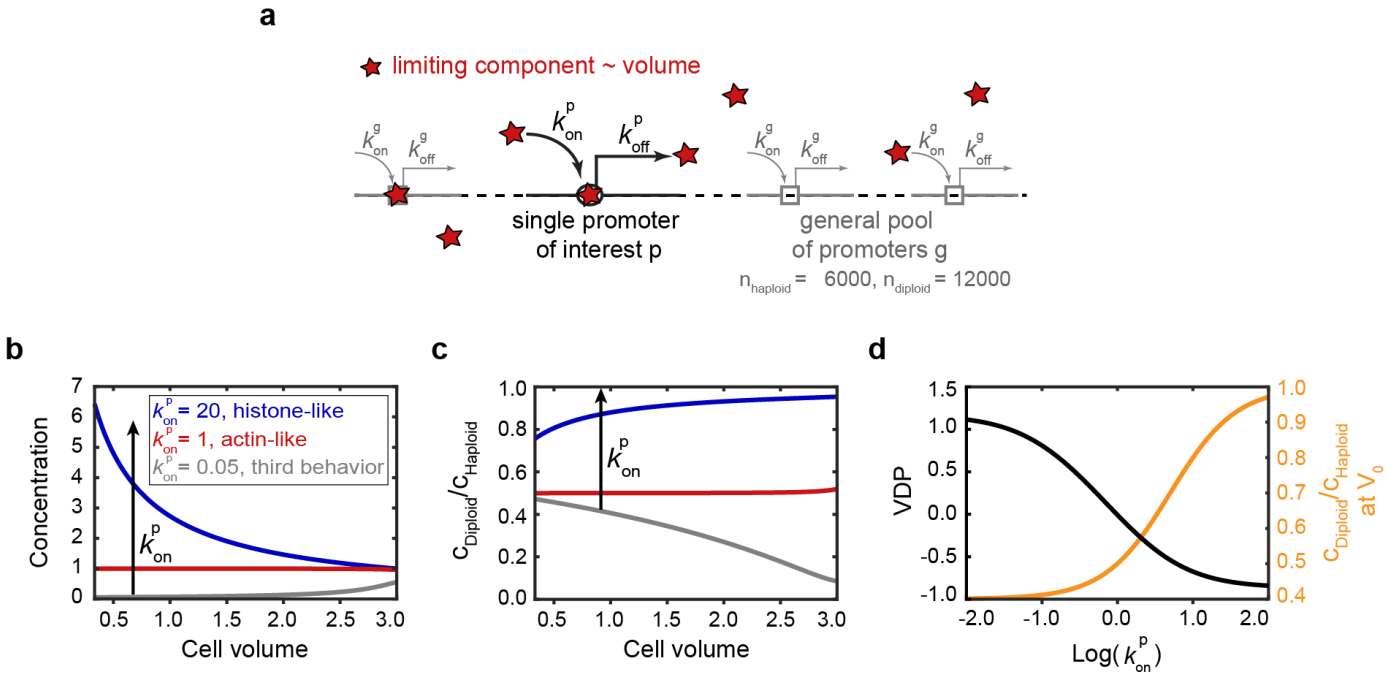

768

769 **Figure 4.** Minimal model for the dependence of transcription rate of one specific promoter of interest
770 on cell volume and ploidy. (a) The model includes two classes of promoters: the general pool of
771 promoters g and the specific promoter of interest p with their respective initiation rates k_{on}^{p} or k_{on}^{g},
772 describing the binding of the limiting machinery and off-rates k_{off}^{p} or k_{off}^{g}, summarizing all other
773 steps of transcription. (b - d) The model predicts that tuning k_{on}^{p} while keeping all other parameters
774 fixed ($c_{TM} = 2000, k_{on}^{g} = 1, k_{off}^{g} = k_{off}^{p} = 3$) results in a qualitative change of the cell volume-
775 dependence of transcript concentration obtained from the specific promoter (b), as well as a change
776 in the ratio between the concentration in diploid cells and the concentration in haploid cells (c). (d)
777 Model prediction for the VDP (right, black) and the ratio between the concentration in diploid cells
778 and the concentration in haploid cells at a characteristic volume $V_0 = 1$ (left, orange) as a function of
779 k_{on}^{p}.

780

bioRxiv preprint doi: https://doi.org/10.1101/2020.08.28.272492; this version posted August 29, 2020. The copyright holder for this preprint (which was not certified by peer review) is the author/funder, who has granted bioRxiv a license to display the preprint in perpetuity. It is made available under aCC-BY-NC-ND 4.0 International license.

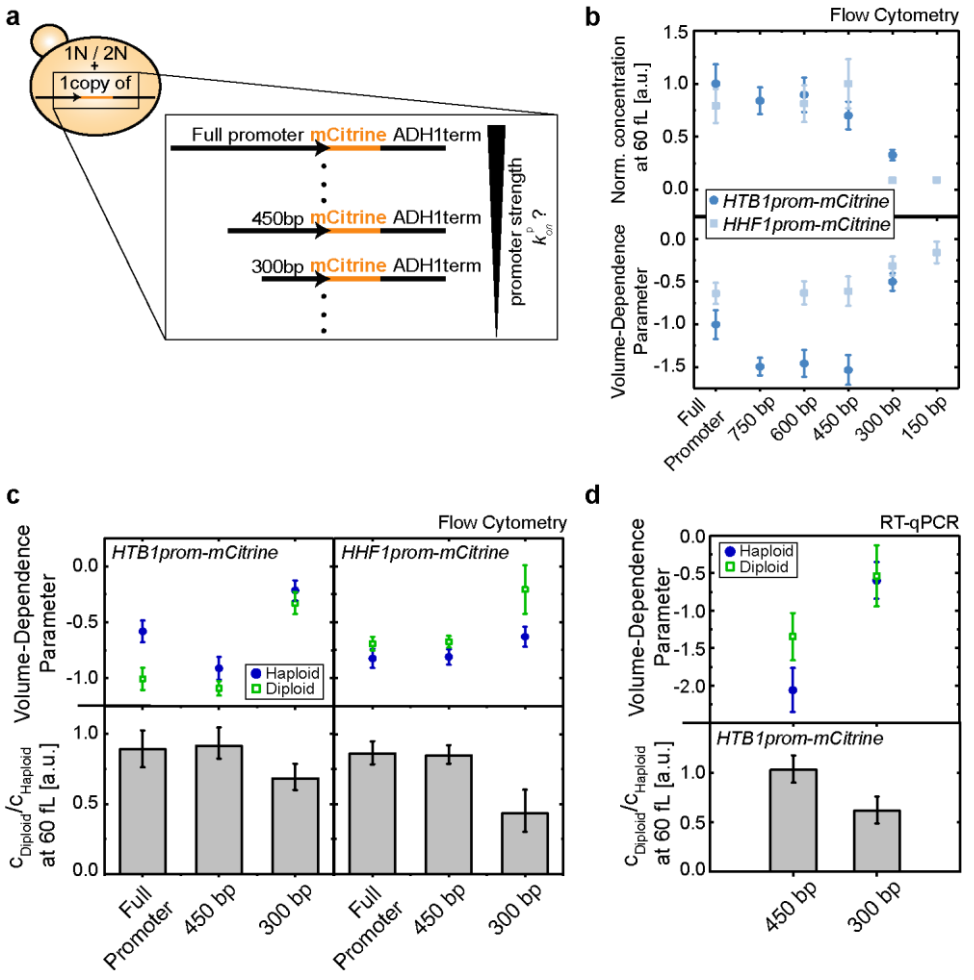

781

782 **Figure 5.** Reducing the strength of a histone promoter shifts its behavior from histone-like to actin-
783 like. (a) Illustration of a series of haploid and diploid strains carrying a single additional copy of
784 increasingly shorter fragments of promoters driving *mCitrine* expression, each truncated from the 5'-
785 end. (b) mCitrine concentration at 60 fL normalized on maximum concentration of the respective
786 promoter (upper panel) and VDP of mCitrine (bottom panel) determined by flow cytometry for the
787 respective promoter truncations of the *HTB1* promoter (dark blue ●) and the *HHF1* promoter (light
788 blue ■) driving *mCitrine* expression, integrated in haploid cells. Error bars in the upper panel are
789 derived by error propagation of the 95% confidence interval of the linear fit at 60 fL. In the bottom
790 panel, error bars show the standard error. (c) VDP of mCitrine in haploid (blue ●) and diploid (green
791 □) cells (upper panel) and mCitrine concentration at 60 fL in diploids compared to the concentration
792 in haploids (bottom panel) determined by flow cytometry. Left shows results for the *HTB1* promoter

bioRxiv preprint doi: https://doi.org/10.1101/2020.08.28.272492; this version posted August 29, 2020. The copyright holder for this preprint (which was not certified by peer review) is the author/funder, who has granted bioRxiv a license to display the preprint in perpetuity. It is made available under aCC-BY-NC-ND 4.0 International license.

793 truncations, right shows results for the *HHF1* promoter truncations. Error bars in the upper panels
794 show the standard error. In the bottom panel, error bars indicate the 2.5- and 97.5-percentiles
795 determined from 10000 bootstrap samples. (d) VDP of *mCitrine* in haploid (blue ●) and diploid
796 (green □) cells (upper panel) and *mCitrine* mRNA concentration at 60 fL in diploids compared to the
797 concentration in haploids (bottom panel) determined by RT-qPCR for *HTB1* promoter truncations
798 driving *mCitrine* expression. Error bars in the upper panel show the standard error. Error bars in the
799 bottom panel indicate the 2.5- and 97.5-percentiles determined from 10000 bootstrap samples.

800

801

802

803

804

805

806

807

808

809

810

811

812